Journal of Nuclear Materials 402 (2010) 8–14

Contents lists available at ScienceDirect

Journal of Nuclear Materials

journal homepage: www.elsevier.com/locate/jnucmat

Microstructural analysis of as-processed U–10 wt.%Mo monolithic fuel plate in AA6061 matrix with Zr diffusion barrier

E. Perez [a], B. Yao [a], D.D. Keiser Jr. [b], Y.H. Sohn [a,*]

[a] Advanced Materials Processing and Analysis Center, Department of Mechanical, Materials and Aerospace Engineering, University of Central Florida, Orlando, FL 32816, USA
[b] Nuclear Fuels and Materials Division, Idaho National Laboratory, Scoville, ID 83415, USA

ARTICLE INFO

Article history:
Received 9 February 2010
Accepted 14 April 2010

ABSTRACT

For higher U-loading in low-enriched U–10 wt.%Mo fuels, monolithic fuel plate clad in AA6061 is being developed as a part of Reduced Enrichment for Research and Test Reactor (RERTR) program. This paper reports the first characterization results from a monolithic U–10 wt.%Mo fuel plate with a Zr diffusion barrier that was fabricated as part of a plate fabrication campaign for irradiation testing in the Advanced Test Reactor (ATR). Both scanning and transmission electron microscopy (SEM and TEM) were employed for analysis. At the interface between the Zr barrier and U–10 wt.%Mo, going from Zr to U(Mo), UZr_2, γ-UZr, Zr solid-solution and Mo_2Zr phases were observed. The interface between AA6061 cladding and Zr barrier plate consisted of four layers, going from Al to Zr, $(Al, Si)_2Zr$, $(Al, Si)Zr_3$ $(Al, Si)_3Zr$, and $AlSi_4Zr_5$. Irradiation behavior of these intermetallic phases is discussed based on their constituents. Characterization of as-fabricated phase constituents and microstructure would help understand the irradiation behavior of these fuel plates, interpret post-irradiation examination, and optimize the processing parameters of monolithic fuel system.

1. Introduction

The Reduced Enrichment for Research and Test Reactor (RERTR) program was created about 30 years ago to develop low-enriched uranium (LEU) plate-type fuels to replace highly enriched uranium (HEU) fuels being used in research and test reactors [1]. Uranium-silicide dispersion fuels, with a uranium-density of around 4.8 g/cm^3, have been previously developed and successfully employed to convert reactors from HEU fuel to LEU fuel [1]. In a dispersion fuel, the fuel meat, comprised of U-bearing fuel particles dispersed in an Al matrix, is clad in AA6061 to form a relatively thin fuel plate. Other higher uranium-density dispersion fuels using U–Mo alloys are currently being developed for the conversion of additional reactors [2]. U–Mo dispersion fuels have been fabricated with a U density of up to 8.5 g U/cm^3 [3]. Some reactors will require a higher U loading in the fuel meat than can be provided by a U–Mo dispersion fuel [4]. As a result, a fuel design is currently being examined so that a higher U loading can be achieved. This fuel type replaces the fuel meat of the dispersion fuel with a monolithic foil of U–10 wt.%Mo alloy (U–10Mo). One performance challenge to be resolved for the monolithic fuel type is the negative impact that foil/cladding chemical interactions in U–Mo–Al system can have during fuel plate irradiation [5]. This interaction can result in the development of a layer at the interface that can develop porosity and deteriorate the foil/cladding bonding. As a result, a Zr diffusion barrier has been added to the fuel design in order to eliminate this interaction at the foil/cladding interface [4]. What particularly makes Zr an effective barrier is the fact that any interactions that do occur between the Zr and U–10Mo and AA6061 during fabrication and irradiation have been observed to be very slow, and more importantly, any interaction products that are formed appear to be stable during irradiation [6].

The starting microstructure of a fuel plate will play a role in determining how the fuel plate will behave during irradiation. Furthermore, in order to adequately interpret the post-irradiation examination results of a fuel plate, a good understand of the starting microstructure is imperative. This paper reports the first electron microscopy characterization results for a monolithic fuel plate with a Zr diffusion barrier that was fabricated as part of a plate fabrication campaign for irradiation testing in the Advanced Test Reactor (ATR). The characterization was performed using scanning electron microscopy (SEM) and transmission electron microscopy (TEM). Of particular interest was the microstructure at the interface between the U–10Mo alloy foil and Zr and between the Zr and the AA6061 cladding. Phase constituents and microstructure that developed during fuel plate fabrication are presented and discussed with respect to their impact on the irradiation performance of a fuel plate.

* Corresponding author. Tel.: +1 407 882 1181; fax: +1 407 882 1461.
E-mail address: ysohn@mail.ucf.edu (Y.H. Sohn).

0022-3115/$ - see front matter © 2010 Elsevier B.V. All rights reserved.
doi:10.1016/j.jnucmat.2010.04.016

2. Relevant phase equilibria and diffusion

In the U–Zr system, the α-U, β-U, γ-UZr, γ_1-U, γ_2-U, δ-UZr_2, α-Zr, β-Zr equilibrium phases exist [7–12]. In addition, transient intermediate phases, monoclinic-α″, martensitic-α′ and hexagonal-ω Zr may develop upon rapid quenching [13,14]. The work of Farkas et al. [15] is of particular interest to this study because they considered the ternary phase equilibrium in a selected region of the U–Zr–Mo system. The α-U, γ-U(Zr), γ-U(Mo), δ-U_2Mo, δ-UZr_2, and $ZrMo_2$ were observed and reported in UZr_2–U_2Mo pseudo-binary phase diagram. They found limited solubility (1–1.5 at.%) of Zr and Mo in δ-U_2Mo and δ-UZr_2 phases, respectively. Rough et al. [16] found that the stability of δ-UZr_2 phase is significantly reduced by oxygen and/or nitrogen contamination. Akabori et al. [17] carried out a diffusion study in U–Zr system with 68, 75 and 78 at.% Zr between 773 and 1023 K. Their study was in agreement with a study conducted by Ogata et al. [18] at higher temperature. However at lower temperature, Ogata et al. [18] reported a reduction in the rates of interdiffusion due to the formation of δ-phase.

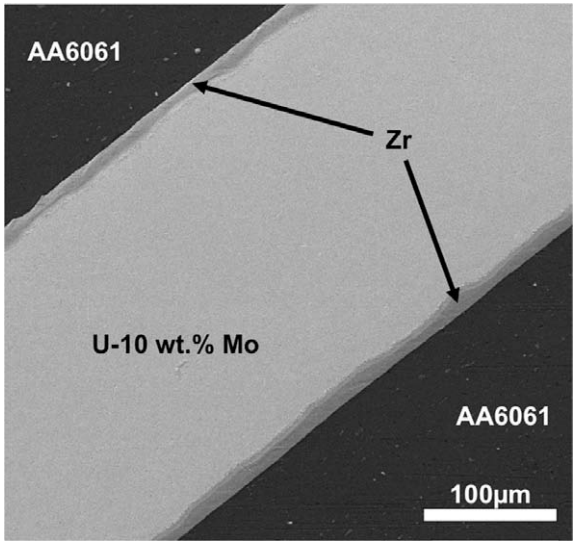

Fig. 1. Backscatter electron micrograph of a monolithic U–10 wt.%Mo fuel plate clad in AA6061 with a Zr diffusion barrier.

The Zr–Al phase diagram [19–21] shows 10 intermetallic compounds, viz. Zr_3Al, Zr_2Al, Zr_5Al_3, Zr_3Al_2, Zr_4Al_3, Zr_5Al_4, ZrAl, Zr_2Al_3, $ZrAl_2$ and $ZrAl_3$. These compounds are all essentially line compounds. Kidson and Miller [22] have studied the chemical diffusion between Zr and Al using bulk diffusion couples in the temperature range of 826–913 K for a maximum of 144 h and reported the formation of only $ZrAl_3$. Gukelberger and Steeb [23] have studied the interdiffusion between Zr and Zr_2Al_3 in the temperature range 1273–1573 K and reported the formation of Zr_5Al_3, Zr_3Al_2 and Zr_4Al_3. Laik et al. [24] annealed a set of Al vs. Zr diffusion couples in the temperature range 838–898 K and observed the development of the $ZrAl_3$. A second layer of Zr_2Al_3 phases was observed at and above 873 K. The observed phase constituents were described based on the modified heat of formation (MEHF) model [25] based on thermodynamic information.

Ten different phases are observed in the equilibrium phase diagram of the Si–Zr system. At the temperatures relevant to this study, the Si–Zr binary phase diagram [26] shows the presence of Si_2Zr, α-SiZr, α-Si_4Zr_5, Si_2Zr_3, $SiZr_2$, $SiZr_3$ phases with very limited solid solubilities. A study of the Al–Zr–Si system was carried out by Jain and Gupta [27] using diffusion couples of solid Zr in contact with liquid phase Al–Si alloys of eutectic composition from 700 to 1100 °C. The $ZrAl_3$, $ZrAl_2$, Zr_2Al_3, Zr_3Al, and ZrSi were observed at 700 °C. At higher temperatures, the ZrAl, Zr_2Al and Zr_3Al, Zr_4Al_3, Zr_5Al_3, Zr_5Al_4 and $ZrSi_2$ phases were observed. Three ternary phases, labeled τ_1, τ_2 and τ_3 were identified. The τ_1 phase was observed throughout the temperature range studied, and had a composition that varied between 9 and 12.6 Si, 23.3 and 25.5 Zr, balance Al (at.%). The τ_2 and τ_3 phases were observed at and above 900 °C. The τ_2 phase, also observed by Schob et al. [28], is a Zr-rich phase with 40.1–42.1 Si, 11.2–11.3 Al, balance Zr (at.%) composition. The τ_3 has a $Zr_3Al_4Si_5$ stoichiometric composition. Jain and Gupta [27] also reported that the Al–Zr binary intermetallic phases have little solubility (1–1.5 at.%) for Si.

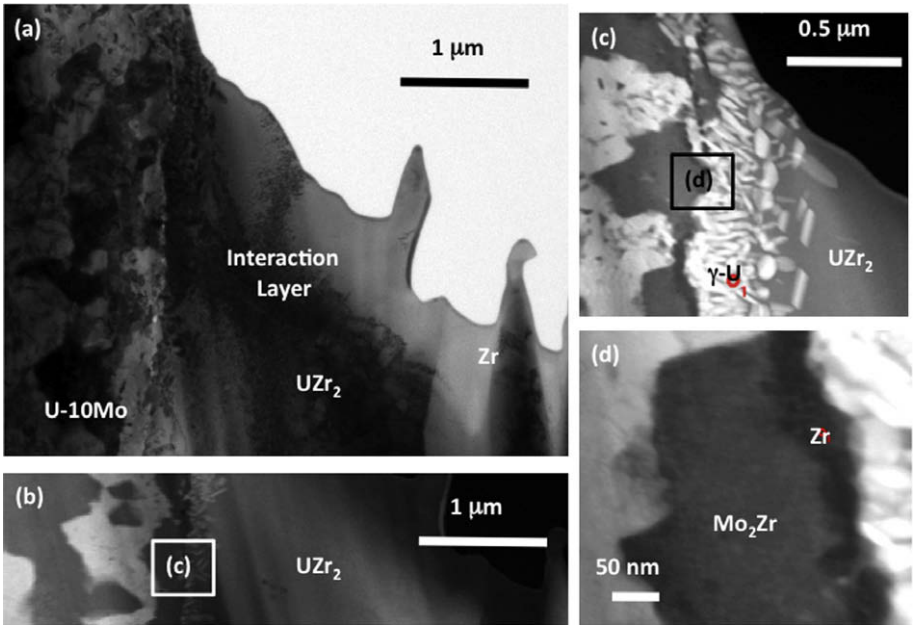

Fig. 2. (a) Bright-field TEM micrograph of the interaction layer that developed between U–10 wt.%Mo fuel plate and Zr diffusion barrier; (b) HAADF TEM micrograph of a selected region; (c) detailed HAADF micrograph of the region labeled "C" in (b); and detailed HAADF micrograph of the region labeled "D" in (c).

3. Experimental procedure

The U–10 wt.%Mo alloy used in this study was cast by arc-melting high purity (>99.9% pure) depleted U and Mo under an Ar atmosphere. The alloy was cast into coupon shape ingots with approximate dimension of 38 mm × 25 mm × 3 mm. The ingots were then laminated, in a carbon steel can, with pure Zr (99.9% pure) foil on each surface. The thickness of the Zr foil was approximately 250 μm before rolling. In order to remove the residual oxide scale on the Al alloy, the AA6061 cladding was etched using 2 M NaOH rinse followed by pickling using 30% nitric acid. Prior to rolling, the assembly was placed in a box furnace that was preheated to 650 °C. Typically 20–40 rolling passes at 650 °C were required to reach the final desired U–10Mo foil thickness of 0.25 mm,

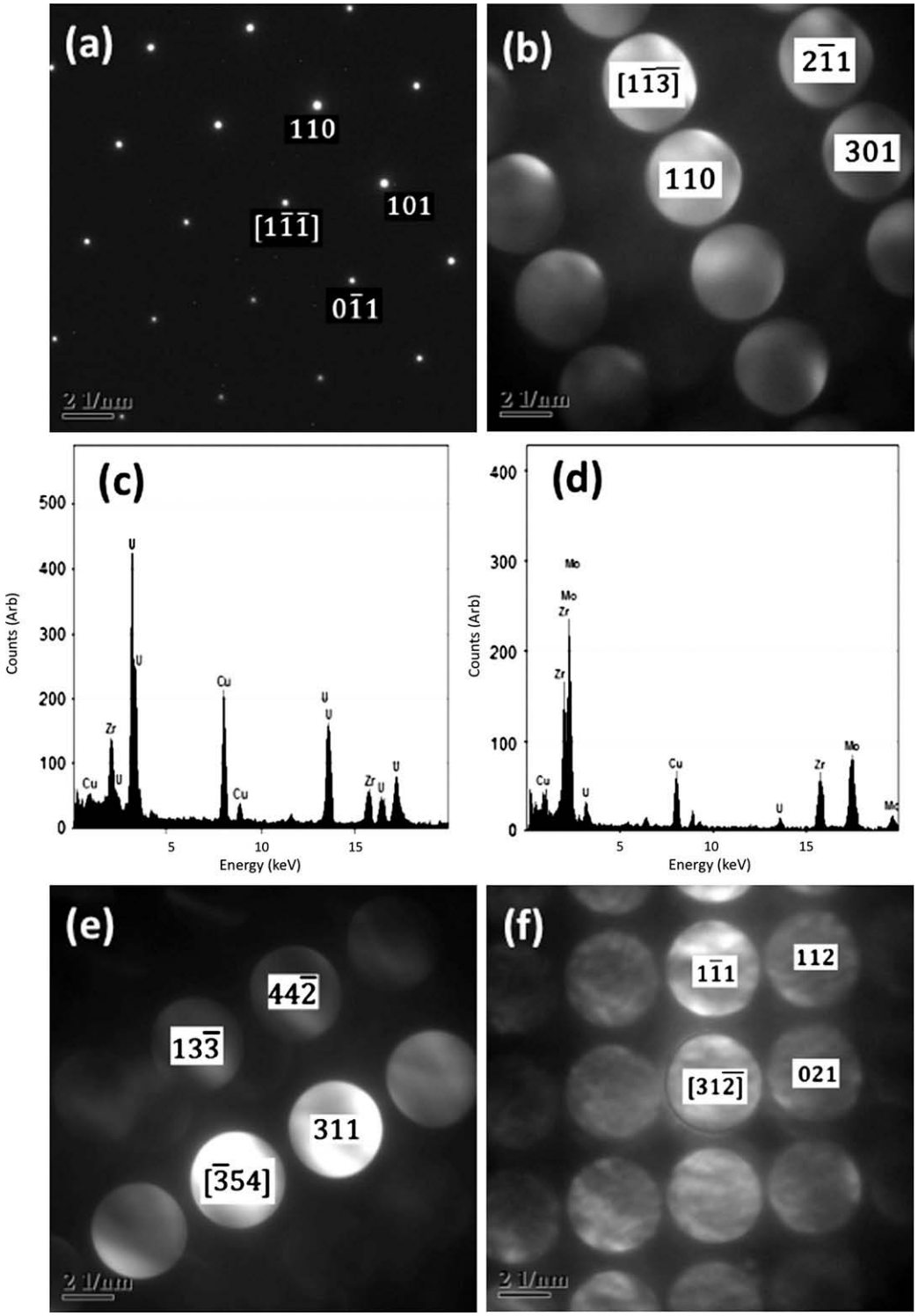

Fig. 3. Typical results from analytical TEM of interaction layer that developed between U–10 wt.%Mo fuel plate and Zr diffusion barrier: (a) SAED pattern from UZr_2 phase; (b) CBED pattern from Zr stabilized γ-U (bcc); (c) XEDS from Zr stabilized γ-U (bcc); (d) XEDS from Zr layer between Mo_2Zr and γ-U (bcc) layers; (e) CBED pattern from Mo_2Zr; and (f) CBED pattern from the transformed α-U.

with a final thickness of around 25 μm for the Zr diffusion barrier. The total time exposed to 650 °C was estimated at approximately 300 min. The assembly was then removed from the can, and cleaned with a mixture of nitric and hydrofluoric acid (2.5% HF, 35% HNO_3 and 62.5% H_2O). Further, to ensure the adhesion among U–Mo, Zr and 6061Al, they were stacked in a hot isostatic press (HIP) stainless steel can with tool steel strong-backs. They were vacuum de-gased at 315 °C for 3 h. The HIP can was then crimp welded and hot isostatic pressed at 560 °C for 90 min at 100 MPa, with a heating and cooling rate of 280 °C per hour.

After the assembly procedure was completed, the fuel assembly with Zr diffusion barrier was sectioned, mounted in epoxy and polished down to 0.25 μm metallographically. General microstructural features of the fuel assembly were examined by using Hitachi 3500 N scanning electron microscopy (SEM) equipped with solid-state backscatter electron (BE) and X-ray energy dispersive spectroscopy (XEDS) detectors. Interface between U–Mo and Zr as well as Zr–Al, where the interdiffusion-induced interaction have taken place, were further examined by FEI/TecnaiTM F30 300 keV TEM equipped with a Fischione™ high angle annular dark field (HAADF) detector and XEDS. Site-specific specimens were prepared by using a FEI TEM200 Focus Ion Beam (FIB) in situ lift-out (INLO) technique. The standardless semi-quantitative XEDS was employed for composition estimation, and selected area electron diffraction (SAED), convergent beam electron diffraction (CBED) and high resolution TEM images were employed to identify the phase constituents.

4. Results

Fig. 1 presents a typical backscatter electron micrograph of the specimen produced according to the process described in Section 3. The light gray region in the middle is the U–10 wt.%Mo monolithic fuel, the dark gray region around is the AA6061 alloy and the intermediate gray layer between these constituents is the Zr barrier plate whose final thickness was approximately 25 μm.

The interface between the U-alloy and Zr, and the Zr and AA6061 alloy was further examined by TEM with specimen preparation by FIB-INLO. Fig. 2 presents (a) bright-field and (b) HAADF micrographs taken from the interface between U–10 wt.%Mo and Zr diffusion barrier. The major constituent of the interaction layer consisted of a continuous 2 μm-thick UZr_2 phase that was in contact with the Zr barrier plate. A SAED pattern from the UZr_2 phase is presented in Fig. 3a. Three other phases were observed upon further examination of the interfacial region between the UZr_2 phase and U–Mo alloy. In Fig. 2c, a detailed HAADF micrograph is presented (i.e., square box labeled "c"). Immediately next to the UZr_2 phase, γ-U (bcc) stabilized with Zr, with a noticeable depletion of Mo, was observed in the matrix of the UZr_2 phase, as shown in Fig. 2c. This two-phase layer was approximately 0.5 μm in thickness. CBED pattern and XEDS data from this γ-U (bcc) phase is presented in Fig. 3b and c. High resolution HAADF micrograph of the region (d) in Fig. 2c is presented in Fig. 2d. A 50 nm-thin layer of relative pure Zr was observed, and its XEDS data is presented in Fig. 3d. However, this layer was too thin to obtain reliable diffraction data. A continuous yet non-planar layer of Mo_2Zr was observed between the pure Zr and U–10 wt.%Mo. A CBED pattern from this phase is presented in Fig. 3e. Its thickness varied from

Table 1
Crystal structures, lattice parameters and space group numbers for relevant phases.

Phases	Structure	Lattice parameters of unit cell (Å)	Space group #
Al	Cubic	4.05 × 4.05 × 4.05	225
$(Al, Si)_3Zr$	Tetragonal	4.01 × 4.01 × 17.29	139
$(Al, Si)_2Zr$	Hexagonal	5.28 × 5.28 × 8.75	194
$(Al, Si)Zr_3$	Cubic	4.37 × 4.37 × 4.37	221
$AlSi_4Zr_5$	Orthorhombic	3.77 × 9.99 × 3.71	63
UZr_2	Hexagonal	5.03 × 5.03 × 3.08	191
Mo_2Zr	Cubic	7.59 × 7.59 × 7.59	227
α-U	Orthorhombic	2.85 × 5.87 × 4.96	63
γ-U	Cubic	3.53 × 3.53 × 3.53	229

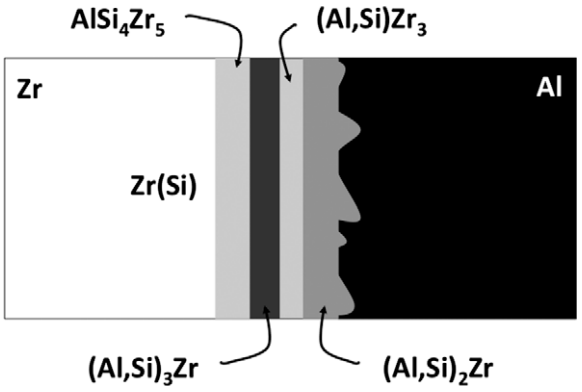

Fig. 5. A schematic representation of microstructure at the interface between a Zr diffusion barrier and AA6061 cladding alloy.

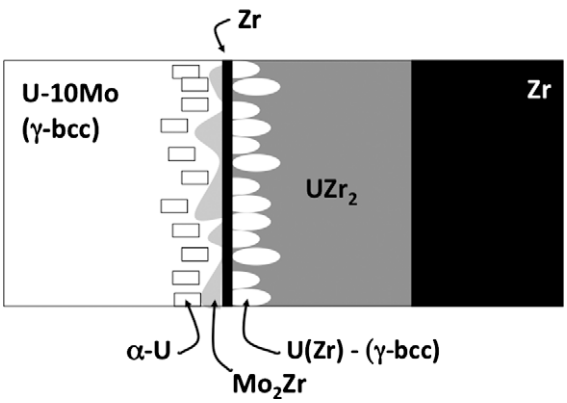

Fig. 4. A schematic representation of microstructure at the interface between a U–10 wt.%Mo fuel plate and Zr diffusion barrier.

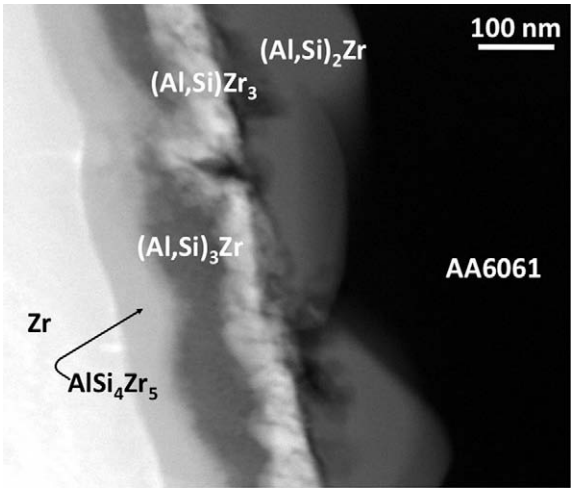

Fig. 6. HAADF micrograph of the interaction layer that developed between Zr diffusion barrier and AA6061 cladding alloy.

a few nm to 250 nm as shown in Fig. 2d. While the bulk of the U–10 wt.%Mo remained as the γ-U (bcc) phase, the region near the interaction layer contained α-U, whose CBED pattern is presented in Fig. 3f. A schematic summary of the interaction layer between U–10 wt.%Mo and Zr barrier plate is presented in Fig. 4, and the crystallographic information on the phases observed in this study is listed in Table 1.

The interface between AA6061 cladding and Zr barrier plate consisted of four layers, $(Al, Si)_2Zr$, $(Al, Si)Zr_3$ $(Al, Si)_3Zr$, and $AlSi_4Zr_5$, from the side of AA6061 to the Zr side. A schematic presentation of the interaction between AA6061 and Zr barrier plate is presented in Fig. 5. The crystallographic information on the phases observed in this study is listed in Table 1, and the HAADF micrograph of the interaction layers is presented in Fig. 6. Typical analytical TEM results, including CBED and HR-TEM micrograph used for phase identification of $(Al, Si)_2Zr$, $(Al, Si)Zr_3$ $(Al, Si)_3Zr$, and $AlSi_4Zr_5$ are presented in Fig. 7 a–d, respectively. The Si in AA6061 was always present in the interaction layers and a significant amount (up to 2 wt.%) was observed within the Zr solid-solution.

5. Discussion

The phases that develop during reactive diffusion can be strongly influenced by the thermodynamic and kinetic properties of each constituent element. At the interface between U–10Mo alloy and Zr barrier, δ-UZr_2 is most likely to be the first phase to develop in the interdiffusion zone, judged by a much thicker layer compared to other products. Since Mo has a very limited solubility (1–1.5 at.%) in δ-UZr_2 [15] and in α-Zr phase [30], the growth of δ-UZr_2 takes place by the consumption of U and Zr, yielding a Mo-rich layer between δ-UZr_2 and U–10Mo. This Mo-rich layer may readily react with Zr atoms, that diffuse through the δ-UZr_2 from Zr cladding layer, to form the Mo_2Zr, the only stable intermetallic alloy between Mo and Zr. It is also suspected that the continuous growth of Mo_2Zr takes place by consumption of Mo from the γ-U phase, resulting in destabilization of this phase. This may explain the presence of the small fraction of α-U phase that was observed between the Mo_2Zr and γ-U layers. Aforementioned, up to eight intermetallic phases can form between Zr and Al, while the

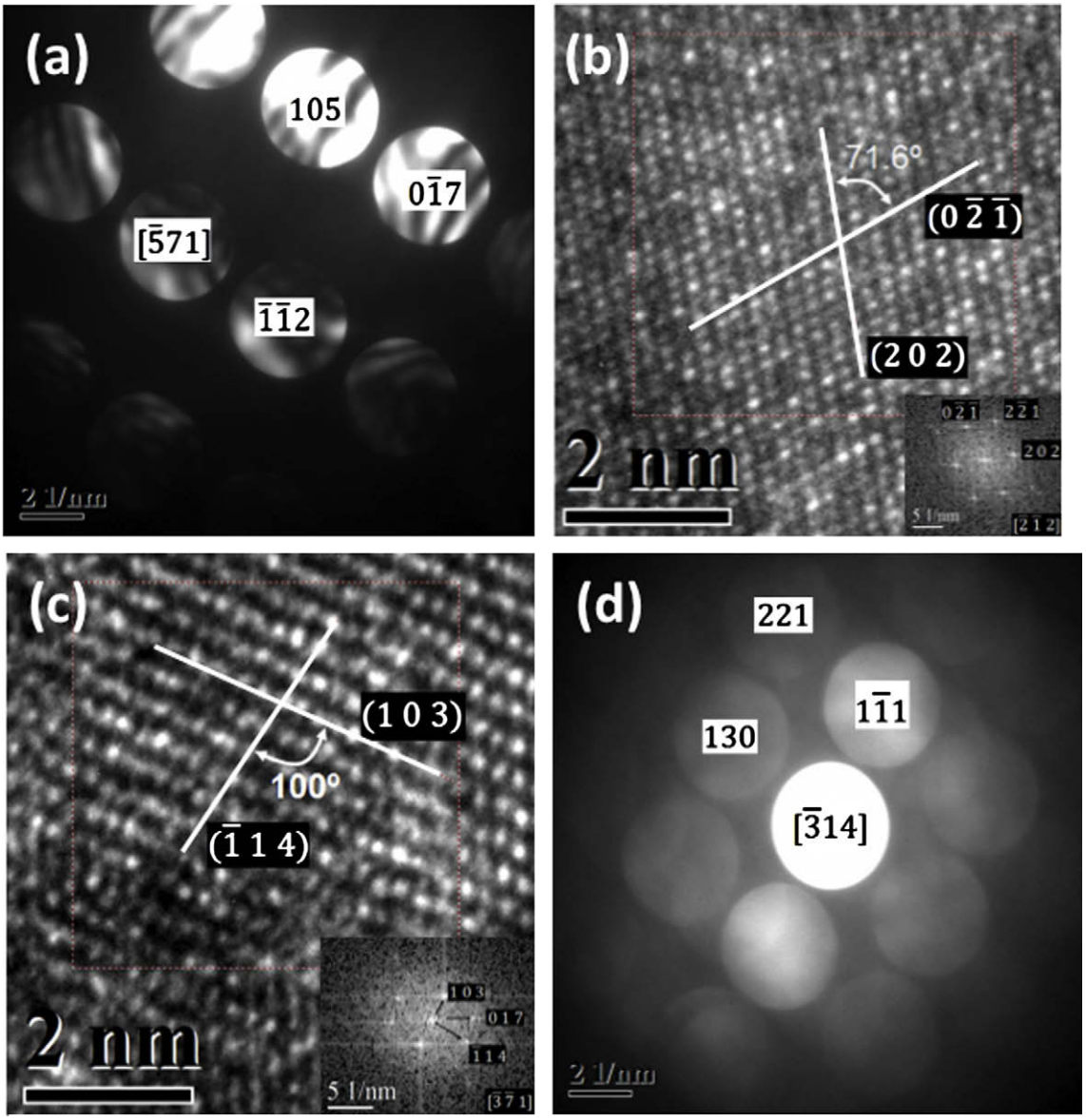

Fig. 7. Typical results from analytical TEM of interaction layer that developed between Zr diffusion barrier and and AA6061 cladding alloy: (a) CBED pattern from $(Al, Si)_2Zr$ phase; (b) HR-TEM image from $(Al, Si)Zr_3$ phase; (c) HR-TEM image from $(Al, Si)_3Zr$ phase; and (d) CBED pattern from $AlSi_4Zr_5$ phase. Inserts within (b) and (c) are the Fast-Fourier-Transformation (FFT) of the corresponding HR-TEM images.

presence of Si within AA6061 Al alloy makes the reactive diffusion and phase evolution more complex. All phases formed in the interaction zone of AA6061 and Zr layers contain significant amounts of Si, which indicates that Si diffuses faster than Al in the interdiffusion zone, and can readily react with the Zr and Al to develop binary compounds with Si dissolved-in and Si-containing ternary compound.

The purpose of incorporating a Zr layer between the U–10Mo and AA6061 cladding in U–10Mo monolithic fuel plates is to eliminate the interaction between the U–10Mo and AA6061 during fabrication and irradiation. This is because the phases that develop in this type of interaction zones do not exhibit acceptable irradiation performance [5]. Based on the results reported in this paper, Zr is acting as an effective diffusion barrier in that no phases containing U, Mo and Al are observed anywhere. This ensures that none of the U–Mo–Al ternary phases that have exhibited poor irradiation performance in the past will be present in the fuel plate with Zr barrier [31].

However, fuel plates with a Zr diffusion barrier develop interaction zones with phases that are different than those observed in fuel plates with only U–10Mo foil and AA6061 cladding. These interaction zones, between U–10Mo with Zr and interaction of the Zr with the AA6061 cladding, form because of the exposure to high temperatures during the fabrication process. The total thicknesses of these zones that form at the U–10Mo/Zr and Zr/AA6061 interfaces are on the order of a few micrometers. In order for a monolithic fuel plate with a Zr diffusion barrier to exhibit the necessary irradiation performance, it is important that the phases in these interaction zones remain stable during irradiation (e.g., low swelling rate). Unstable behavior of these phases could result in the development of porosity at the U–10Mo/Zr and Zr/AA6061 interfaces that could result in de-bonding of the U–10Mo fuel foil with the AA6061 cladding and premature failure of the fuel plate.

The most prevalent phase at the interface between U–Mo and Zr was observed to be UZr_2, whose irradiation behavior in sodium fast reactors has been documented by Hofman and Walters [29]. U–Zr alloys have typically been irradiated at higher temperatures than the monolithic fuels discussed in this paper. The good irradiation behavior of the UZr_2, which has been reported at high temperatures in U–Zr alloys [29], must be demonstrated at the lower irradiation temperatures seen by U–Mo monolithic fuel plates with a Zr barrier. This behavior will be investigated through irradiation testing in the Advanced Test Reactor.

The interaction between U–10 wt.%Mo and Zr also produced the α-U phase, and the irradiation behavior for this phase is not expected to be as good as for the UZr_2 phase. In general, γ-phase uranium alloys, with a bcc crystal structure, exhibit more stable irradiation behavior than α-U phase with an orthorhombic crystal structure [29]. However, due to the small amount of α-U that is present, the overall impact on the irradiation behavior of the fuel plate should be negligible.

The interaction at the Zr/AA6061 cladding interface produced, from AA6061 to the Zr, $(Al, Si)_2Zr$, $(Al, Si)Zr_3$ $(Al, Si)_3Zr$, and $AlSi_4Zr_5$ phases. During the nuclear fission process, irradiation damage can take place in a recoil zone that can extend from the U–10Mo fuel into the Zr or Al for a distance of about 10 μm [32]. The fission fragments and thermal spikes within the recoil zone produce the damage, and similar irradiation damage has resulted in the amorphization of some phases found in the U–Mo–Al and U–Mo–Al–Si systems [33,34]. Similarly, this damage may affect the crystallinity of those phases observed at the U–10Mo/Zr interface. However, those phases identified at the Zr/AA6061 interface should not be contained in the recoil zone of the U–10Mo foil since the Zr diffusion barrier is at least 25 μm thick, and as a result, these phases should not go amorphous. Therefore, only the behavior of crystalline phases at this interface will have to be considered when evaluating the irradiation performance of a U–Mo monolithic fuel plate with Zr diffusion barrier.

In the future, it will be critical to characterize additional monolithic fuel plates that contain a Zr diffusion barrier, preferably using TEM, since any changes in the materials (e.g., impurity contents) or how the fuel plates are fabricated (e.g., time at temperature) will affect the phases and microstructure that are present at the U–10Mo/Zr and Zr/AA6061 interfaces. The presence of different phases or different amounts of phases can have varying effects on the overall irradiation performance of a fuel plate.

6. Summary

Microstructural characterization of a monolithic U–10 wt.%Mo fuel plate clad in AA6061 with a Zr diffusion barrier was carried out by SEM and TEM. The UZr_2, γ-UZr, Zr solid-solution and Mo_2Zr phases were observed at the interface between the Zr barrier and U–10 wt.%Mo. Layers of $(Al, Si)_2Zr$, $(Al, Si)Zr_3$ $(Al, Si)_3Zr$, and $AlSi_4Zr_5$ were observed at the interface between AA6061 cladding and Zr barrier plate. The phase constituents and their amounts observed appear promising for positive irradiation performance.

Acknowledgements

This work was financially supported by Idaho National Laboratory (Contract No. 00051953) under the operation of US Department of Energy, Office of Nuclear Materials Threat Reduction (NA-212), National Nuclear Security Administration, under DOE-NE Idaho Operations Office Contract DE-AC07-05ID14517.

References

[1] J.L. Snelgrove, G.L. Hofman, M.K. Meyer, C.L. Trybus, T.C. Wiencek, Nucl. Eng. Des. 178 (1997) 119–126.
[2] D.D. Keiser Jr., S.L. Hayes, M.K. Meyer, C.R. Clark, Jom 55 (2003) 55–58.
[3] A. Leenaers, S. Van den Berghe, E. Koonen, C. Jarousse, F. Huet, M. Trotabas, M. Boyard, S. Guillot, L. Sannen, J. Verwerft, Nucl. Mater. 335 (2004) 39–47.
[4] Daniel Wachs et al., Progress in the development of LEU fuel, in: Proceedings of the GLOBAL'07 International Conference on Advanced Nuclear Energy and Fuel Cycle Systems, Boise, ID, September 9–13, 2007.
[5] D.D. Keiser Jr., A.B. Robinson, M.R. Finlay, Observations derived from the characterization of monolithic fuel plates irradiated as part of the RERTR-6 experiment, in: Proceedings of the 29th International Meeting on Reduced Enrichment for Research and Test Reactors (RERTR), Prague, Czech Republic, September 23–27, 2007. <http://www.rertr.anl.gov>.
[6] A.B. Robinson, D.M. Wachs, D.E. Burkes, D.D. Keiser, US RERTR fuel development post irradiation examination results, in: Proceedings of the 30th International Meeting on Reduced Enrichment for Research and Test Reactors (RERTR), Washington, D.C., October 5–9, 2008. <http://www.rertr.anl.gov>.
[7] T.B. Massalski (Ed.), Binary Alloy Phase Diagr, ASM Metals Park, OH, 1986.
[8] R.I. Sheldon, D.E. Peterson, Bull. Alloy Phase Diagr 10 (2) (1989) 165.
[9] L. Leibowitz, R.A. Blomquist, A.D. Pelton, J. Nucl. Mater. 167 (1989) 76.
[10] T. Ogawa, T. Iwai, J. Less-Common Met. 170 (1991) 101.
[11] H. Okamoto, J. Phase Equilib. 13 (1) (1992) 109.
[12] H. Okamoto, Phase Diagr. Binary Actin. Alloy (1995) 246.
[13] C. Basak, R. Keswani, G.J. Prasad, H.S. Kamath, N. Prabhu, S. Banerjee, J. Nucl. Mater. 393 (2009) 146.
[14] V.K. Orlov, V.M. Teplinskaya, At. Energy 86 (2) (1999) 118.
[15] M.S. Farkas, A.A. Bauer, F.A. Rough, Trans. Met. Soc. AIME 215 (1959) 685.
[16] F.A. Rough, A.E. Austin, A.A. Bauer, J.R. Doig, Metall. Ceram (M-3679, 17th ed.), (1956) BMI-1092.
[17] M. Akabori, A. Itoh, T. Ogawa, T. Ogata, J. Alloy Compd. 271–273 (1998) 597.
[18] T. Ogata, M. Akabori, A. Itoh, T. Ogawa, J. Nucl. Mater. 232 (1996) 125.
[19] H. Okamoto, J. Phase Equilib. 23 (2002) 455.
[20] A. Peruzzi, J.P. Abraita, Alloy Binary Phase Diagram, second ed., ASM International (1990), p. 241.
[21] Z. Murray, A. Peruzzi, J.P. Abraita, J. Phase Equilib. 13 (1992) 277.
[22] G.V. Kidson, G.D. Miller, J. Nucl. Mater. 1 (1964) 61.
[23] A. Gukelberger, S. Steeb, Z. Metallkd. 69 (1978) 255.
[24] A. Laik, K. Bhanumurty, G.B. Kale, Intermetallics 12 (2004) 69.
[25] R. Pretorius, Mater. Res. Soc. Proc. 25 (1984) 15.
[26] H. Okamoto, Bull. Alloy Phase Diagr. 11 (1990) 513.
[27] J.K. Jain, S.P. Gupta, Mater. Charact. 49 (2003) 139.
[28] O. Schob, H. Nowotny, F. Benesovsky, Monatsh Cem. 92 (1961) 1218.

[29] G.L. Hofman, L.C. Walters, Metallic fast reactor fuels, in: R.W. Cahn, P. Haasen, E.J. Kramer (Eds.), Materials Science and Technology: A Comprehensive Treatment, vol. 10. VCH Publishers Inc., New York, 1994, p. 1.
[30] ASM Handbook, Alloy Phase Diagrams, vol. 3 pp. 1160–1161.
[31] G.L. Hofman, M.R. Finlay, Y.S. Kim, Post-irradiation analysis of low enriched U–Mo/Al dispersions fuel miniplates Tests RERTR-4&5, in: Proceedings of the 26th Int. Meeting on RERTR, November 7–12, 2004, Vienna, Austria.
[32] D. Olander, J. Nucl. Mater. 372 (2008) 94–105.
[33] S. Van den Berghe, W. Van Renterghem, A. Leenaers, J. Nucl. Mater. 375 (2008) 340–346.
[34] J. Gan, D.D. Keiser Jr., D.M. Wachs, A.B. Robinson, B.D. Miller, T.R. Allen, J. Nucl. Mater. 396 (2010) 234–239.